UHASSELT
KNOWLEDGE IN ACTION

Maastricht University

Faculty of Medicine and Life Sciences
School for Life Sciences
Master of Biomedical Sciences

Master's thesis

Guiding the Way: A Refined Echo-Guided Injection Protocol for Intramyocardial Delivery of Therapeutic Agents in a Rat Model of Myocardial Infarction

Rob Simons
Vincent Vandenboer

Thesis presented in fulfillment of the requirements for the degree of Master of Biomedical Sciences, specialization Molecular Mechanisms in Health and Disease

SUPERVISOR :

Prof. dr. Virginie BITO

MENTOR :

Mevrouw Lotte VASTMANS

Mevrouw Ellen HEEREN

2024
2025

Transnational University Limburg is a unique collaboration of two universities in two countries: the University of Hasselt and Maastricht University.

UHASSELT
KNOWLEDGE IN ACTION

www.uhasselt.be
Universiteit Hasselt
Campus Hasselt:
Martelarenlaan 42 | 3500 Hasselt
Campus Diepenbeek:
Agoralaan Gebouw D | 3590 Diepenbeek

Faculty of Medicine and Life Sciences
School for Life Sciences
Master of Biomedical Sciences

Master's thesis

Guiding the Way: A Refined Echo-Guided Injection Protocol for Intramyocardial Delivery of Therapeutic Agents in a Rat Model of Myocardial Infarction

Rob Simons
Vincent Vandenboer

Thesis presented in fulfillment of the requirements for the degree of Master of Biomedical Sciences, specialization Molecular Mechanisms in Health and Disease

SUPERVISOR :

Prof. dr. Virginie BITO

MENTOR :

Mevrouw Lotte VASTMANS

Mevrouw Ellen HEEREN

Guiding the Way: A Refined Echo-Guided Injection Protocol for Intramyocardial Delivery of Therapeutic Agents in a Rat Model of Myocardial Infarction

Vincent Vandenboer[1], Lotte Vastmans[1], Ellen Heeren[1], and Virginie Bito[1]

[1]Cardio & Organ Systems (COST), Biomedical Research Institute, University Hasselt, Campus Diepenbeek
Agoralaan Gebouw C - B-3590 Diepenbeek

*Running title: *New Echo-Guided Injection Method for MI in Rats*

To whom correspondence should be addressed: Virginie BITO, Tel: +32 11 26 92 85; Email: virginie.bito@uhasselt.be

The main chapter of this thesis is part of a manuscript under minor revisions in JoVE (JoVE68775).

Keywords: Myocardial infarction, Echo-guided injection, Rats, Intramyocardial, Bioluminescence

ABSTRACT

Cardiovascular disease (CVD) is the leading cause of death worldwide, with myocardial infarction (MI) accounting for over 80% of CVD-related deaths. MI results from ischemia caused by atherosclerotic plaque formation, leading to inflammation, cell death, fibrosis, and adverse cardiac remodeling. While current therapies, such as pharmacological and percutaneous coronary intervention, restore perfusion, they fail to regenerate the damaged myocardium. As a result, regenerative approaches such as gene and stem cell therapies gain attention, but require accurate peri-infarct delivery. Invasive Open-chest intramyocardial injection is a well-established preclinical model, but lacks repeatability. Echocardiography-guided injection (EGI) offers a minimally invasive repeatable alternative, although it's primarily developed in mice, with limited adaptation for rats. In this study, we present a refined, safe, accurate, and reproducible EGI protocol in a MI rat model. Injections were executed in the parasternal long axis using a 29 G × 88 mm Spinocan® spinal needle, selected for its extra-long shaft and fine bevel to comply with the rat's thoracic anatomy. Accuracy and efficiency were assessed by injection of a Texas-Red dextran tracer and cardiac progenitor cells expressing firefly luciferase, visualized using bioluminescence. Color Doppler imaging validated safety, which showed no excessive bleeding during and after EGI. Fluorescence imaging combined with Sirius Red staining confirmed targeted peri-infarct delivery, while bioluminescence indicated efficiency and cell retention. This protocol provides an optimized, safe, and precise method for intramyocardial EGI injection in a rat model of MI. This approach offers a valuable tool to reduce the gap between pre-clinical research and clinical applications.

INTRODUCTION

CVD remains one of the leading causes of morbidity and mortality worldwide, with an estimated 931 578 deaths annually in 2021 in the United States (1). CVDs are a group of diseases related to the cardiovascular system, including MI. In addition, >80% of the annual deaths are caused by MI and its implications (2). Moreover, 20%-30% of MI diagnosed patients develop heart failure over 1 year, seriously increasing mortality risk (3). MI primarily results from the formation and rupture of atherosclerotic plaques within a coronary artery. This event leads to partial or complete occlusion of the vessel lumen, thereby severely limiting the delivery of oxygenated blood to downstream myocardial tissue. The ensuing hypoxic conditions induce a localized ischemic region within the myocardium, ultimately culminating in cardiomyocyte necrosis. Primarily, the deprivation of oxygen results in apoptosis and necrosis of the affected myocardial cells, followed by an inflammatory response involving macrophages due to cellular damage and debris. Secondly, macrophages undergo a phenotypic switch toward a

regeneration-promoting state, thereby stimulating cardiac fibroblasts to differentiate into myofibroblasts. This leads to the formation of fibrocollagenous scar tissue, a process known as fibrosis, which induces structural remodeling and alters the functional properties of the remaining myocardial tissue (4). Thirdly, adverse cardiac remodeling occurs as a consequence of fibrosis. This phenomenon is characterized by architectural changes such as ventricular enlargement, longitudinal deformation, and a twist in the apex, leading to compensation of cardiac function by the healthy, unaffected myocardium. Ultimately, these changes result in cardiac hypertrophy and decreased cardiac performance. Without timely intervention, these pathological changes can culminate in heart failure (HF), due to the limited regenerative capacity of adult cardiomyocytes (5).

Current therapies rely on managing blood flow and preventing HF following MI through early reperfusion and pharmacological strategies. The minimally invasive percutaneous coronary intervention (PCI) is the reperfusion strategy with the best clinical outcome (6). Invasive coronary bypass grafting remains a reliable reperfusion strategy in PCI-failed patients. In addition to reperfusion, pharmacological therapy plays a critical role both in prevention and in post-MI management. Angiotensin-converting enzyme inhibitors (ACEi), whether or not in combination with beta blockers, are used to decrease blood pressure. On the other hand, mineralocorticoid receptor antagonists and statins could be used to lower blood cholesterol levels and reduce the risk of atherosclerotic plaque deposition. In addition, antithrombotic agents could be used to prevent blood from clotting (6). Even with the outstanding reliability and the high success rate of the currently used therapies, they face a common failure; they lack focus on repairing and, ideally, regenerating the lost cardiac tissue.

Hence, research has progressively shifted its focus toward regenerative medicine to restore the lost myocardium. Some of the most promising new therapeutic approaches include stem cells, such as bone marrow-derived mononuclear cells (BMMNCs), mesenchymal stem cells (MSCs), and induced pluripotent stem cells (iPSCs), amongst others (7). Another innovative treatment is gene therapy, for example, microRNAs (miRNA) or adeno-associated viruses (AAV) to stimulate cardiac function or reverse cardiac dysfunction by specialized delivery of genetic sequences to induce cardiac modulating effects (8). For example, sarcoplasmic/Endoplasmic Reticulum Calcium ATPase 2 (SERCA2) induction by AAV-mediated gene delivery improved contractility and decreased the cardiac remodeling rate in sheep (9). Moreover, miRNAs 1, 133, 208, and 499 showed the ability to transform fibroblasts into cardiomyocyte-like cells expressing the cardiomyocyte phenotype and exhibiting a spontaneous calcium flux *in vitro* in mice (10). However, the promising capacities of these therapies share a common hurdle: the need for precise and accurate delivery in the peri-infarct zone. Creating the need for specialized administration methods.

Currently, several methods are used to deliver these innovative therapies. For example, transendocardial injection (TE), (direct) intramyocardial injection (IM), intravenous injection (IV), and intracoronary injection (IC) (11, 12). In the preclinical setting, IM injection is the most commonly used method, but it comes with an extensive amount of cell leakage after injection. Nevertheless, TE injections in patients and IM injections in swine show promising results in improving ejection fraction (12). Meanwhile, IC and IV injections come with less mechanical stress and are less invasive, but exhibit the risk of trapping the injected cells in other organs like the lungs, kidneys, or liver (11, 13). Moreover, IC and IV injections show inferior preclinical results compared to TE injection and IM injection in swine (12). Clinical studies have demonstrated beneficial outcomes following both TE and IV injections. In contrast, IM injections are limited to patients undergoing surgical PCI, and IC injections have shown only modest improvements (11, 12).

In a clinical setting, IM injections are being performed using injection catheters, which are guided to the peri-infarct zone where precise injection is performed (14). However, this type of injection is not feasible in rodents, due to their small size and the complexity of the procedure.

Rodents like mice and rats are often used in cardiovascular research due to their physiological similarity and low-cost maintenance (15). However, developing a method that closely mimics the techniques used in clinical practice and focuses on the targeted delivery of a regenerative therapy is essential to preserve the translational value from preclinical to clinical research. This consideration brings us the well-established, translational echocardiography-guided injection (EGI) that is frequently used in mouse models of MI (16). Typically, IM injections require an invasive open-chest injection that is accompanied by scarring and adhesion formation, preventing repeated injections and delayed therapeutic delivery, limiting the translational value of preclinical studies (17). These issues can be addressed by using EGI, which represents a safe, minimally invasive alternative for the IM delivery of therapeutics (18). EGI in mice typically involves delivering the therapeutic agent into the left ventricular wall under real-time short-axis (SAX) imaging. This approach minimizes the risk of damaging adjacent organs and avoids the invasiveness of open-chest surgery. However, it presents certain limitations. First, it is challenging to confirm that the needle tip remains entirely within the myocardial tissue throughout the injection. Second, the approach restricts access to certain myocardial regions, limiting the precision with which specific sites can be targeted (16). Although this technique has been well described and optimized for use in mice, clear protocols for its application in rats are lacking. As a result, there is a pressing need for well-defined procedures to enable the reliable implementation of this method in rat models. Moreover, the implementation of EGI in rats introduces additional limitations that must be taken into account. Firstly, the 30 G needles typically used in mice are too short to allow effective IM injection in rats (16). Furthermore, MI leads to thinning of the ventricular wall, which complicates accurate peri-infarct injection. To mitigate this, a fine-gauge needle with a small bevel is required to minimize the risk of perforation and leakage of the injectate. In addition, when injections are performed in the parasternal long axis (PSLAX) imaging, a longer needle shaft is often needed to reliably reach the target region. To address these limitations, an EGI protocol was optimized with the use of a 29 G x 88mm Spinocan® needle to enable safe IM injection. We hypothesize that the refined protocol for IM EGI in a rat model of MI offers a safe and effective method for administering therapeutics, based on Doppler imaging, bioluminescence imaging (BLI), and Texas-Red dextran tracer injection.

EXPERIMENTAL PROCEDURES

Animal experimentation – Animal experimentation was conducted following EU Directive 2010/63/EU and approved by the Local Ethical Committee for Animal Experimentation (UHasselt, Belgium, Diepenbeek; ID 202234K, ID202497). All animals were housed under controlled conditions (humidity: 60%, 21°C) with a 12-hour light-dark cycle and provided with a standard pellet diet and *ad libitum* access to water. A total of 44 female Sprague-Dawley rats (Janvier Labs, Le Genest-Saint-Isle, France) were used in this study: 22 for cell isolation and 20 for EGI experiments.

Optimization and assessment of rCPCs lentiviral transduction – Lentiviruses containing a pLV[Exp]-EF1A>Luciferase(ns)/3xFLAG:T2A: Puro vector (VectorBuilder GmbH, Neu-Isenburg, Germany) encoding for firefly luciferase ($Fluc^+$) and a puromycin resistance gene were used for transduction of rat cardiac progenitor cells (rCPCs). To determine the optimal multiplicity of infection (MOI) for transduction, a combined assay was performed, assessing cell viability after puromycin selection as a proxy for transduction efficiency, alongside luciferase expression as a qualitative measure confirming functional delivery and expression of the luciferase gene by the vector. Therefore, passage one rCPCs were transduced at MOIs of 5, 10, 15, and 25 in 5% FCS-enriched X-Vivo medium with 8 µg/mL polybrene for six hours. Following transduction, cells were cultured in 20% FCS-enriched medium for three days before undergoing puromycin selection (2.5 µg/mL) for 72 hours.

To assess cell viability, alamarBlue™ Cell Viability reagent (Invitrogen, Renfrew, United Kingdom) was used according to the manufacturer's protocol. Following puromycin

selection, the cells were incubated for four hours with 10% alamarBlue™ in fresh medium at 37°C. Then, the supernatant was transferred to a black 96-well plate, and absorbance was measured at 570nm and 600nm using the Clariostar Plus microplate reader (BMG Labtech, Ortenberg, Germany). Viability values were normalized against the positive control (non-transduced cells, not exposed to puromycin), which was set as 100% viability.

To confirm luciferase expression following transduction, luminescence was measured using the One-Glo™ Luciferase Assay System (Promega, Madison, WI, USA) in the same wells following the alamarBlue™ assay. The positive control condition was used as a background reference for luminescence. In addition, a blank (medium plus One-Glo only) was included to assess reagent background. Luminescence was obtained using the Clariostar Plus microplate reader. Relative luminescent units (RLU) were obtained by performing background correction and normalization compared to the positive control.

Transduction of rCPCs for bioluminescence tracking – Lentiviruses carrying the luciferase and puromycin resistance vector described above were used to transduce passage one rCPCs. Cells were transduced at an MOI of 25 in 5% FCS-enriched X-Vivo medium supplemented with 8 µg/mL polybrene for six hours. After transduction, cells were maintained in 20% FCS-enriched X-Vivo medium for three days, followed by puromycin selection at 2.5 µg/mL for 72 hours. After selection, cells were cultured under standard conditions until reaching 80–90% confluency, at which point they were collected for echocardiography-guided injection.

Echocardiography-guided injection (EGI) – EGI was performed one week after induction of myocardial infarction by permanent LAD ligation, as described in Supplementary Methods. Echocardiographic imaging was conducted using a Vevo 3100 Imaging Platform (FUJIFILM VisualSonics, Inc., Amsterdam, The Netherlands) equipped with the MX250 transducer (FUJIFILM VisualSonics, Inc., Amsterdam, The Netherlands). Rats were anesthetized with 2.5-3% isoflurane in oxygen (2 L/min) and received prophylactic buprenorphine 0.04 mg/kg (Richter Pharma AG, Wels, Austria). Anesthesia was maintained with 1-3% isoflurane in 1 to 1.5 L/min oxygen. Body temperature was monitored and maintained at 37 0.5 °C using the integrated heated platform. The infarcted and peri-infarct regions were identified using PSLAX imaging in both B- and M-mode. Once the injection site was determined, the guide needle (Spinocan® BBraun, Brussels, Belgium), mounted on a 1 mL syringe (Terumo, Genk, Belgium), was positioned on the injection stand, ensuring optimal needle-transducer alignment. The guide needle was inserted into the thoracic wall towards the predetermined target region, after which the syringe was detached, leaving the guide needle in place. The 29 G x 88mm Spinocan® (BBraun, Brussels, Belgium) needle was attached to the syringe and introduced through the lumen of the guiding needle towards the target region. Upon echographic visualization of the needle bevel, the guide needle was retracted. The 29 G needle was further advanced for precise IM delivery. Upon clear visualization of the injectate, the needle was slowly retracted to minimize leakage.

Color Doppler imaging for safety assessment during EGI – During EGI procedures, echocardiographic images were captured using the Vevo 3100 Imaging Platform in B-mode PSLAX to visualize needle positioning in relation to cardiac anatomy. Color Doppler imaging was applied in real time to monitor the left ventricle and ventricular wall for signs of procedural complications, such as unintended punctures or blood leakage.

Hydrogel spatial distribution – A dextran Texas-Red 70.000 MW lysin fixable fluorescent (Invitrogen, Renfrew, United Kingdom) tracer embedded in a hydrogel matrix was injected in the peri-infarct zone to assess the spatial distribution of the injectate after EGI. Cardiac tissue was isolated and cut into 3 mm slices. Subsequently, the tissue was embedded in 4% paraformaldehyde overnight and preserved in 30% sucrose at 4°C. Cardiac tissue was embedded in Tissuetec (Leica Biosystems, Diegem, Belgium), and subsequently cryosections of 10µm were obtained using a

Leica cryostat (Leica Biosystems, Diegem, Belgium). Cryocoupes were counterstained using DAPI (1:5000) (Sigma-Aldrich, Overijse, Belgium). Images were acquired using an AxioScan (Zeiss, Zaventem, Belgium) fluorescent imager. Collagen was stained using Sirius Red staining (Chondrex, Woodinville, United States), distinguishing the infarcted region from healthy myocardium.

Bioluminescent imaging - In vivo and *ex vivo* BLI were performed within one hour after $FLUC^+$ rCPC injection. Bioluminescent images were acquired using an IVIS Lumina III bioluminescent imager (PerkinElmer, Massachusetts, United States). Rats were sedated, as described above, and injected with 375 mg/kg d-luciferin intraperitoneally. Subsequently, rats were imaged for 30 minutes with 2-minute intervals. Afterwards, rats were euthanized with an overdose of sodium pentobarbital (Dolethal, Vetoquinol, Aartselaar, Belgium, 200 mg/kg, i.p.), hearts were isolated, cut into 3 mm slices, and imaged *ex vivo*. Bioluminescence was quantified in photons /second.

RESULTS

rCPC transduction efficiency and vector expression increase with rising multiplicity of infection – rCPCs were transduced using lentiviral vectors encoding firefly luciferase and a puromycin resistance gene, enabling antibiotic-based selection of successfully transduced cells. To determine the optimal transduction conditions, rCPCs were transduced with increasing MOIs in 10% and 20% FCS. Cell viability following transduction was assessed using Alamar-Blue reagent, while luciferase expression, used as a measure for vector expression, was quantified using the OneGlow luciferase assay. Both 6h and o/n transduction showed increasing relative viability for increasing MOIs, indicating an optimal MOI of 20-25. However, no relevant difference could be observed between transduction in 10% FCS and 20% FCS (**Fig. 1A-1B**). In relation to the vector expression, a higher MOI could be related to an increase in fold change of the RLU signal, indicating more vector expression (**Fig. 1C**).

Set-up overview, animal positioning, and echocardiographic imaging - A frontal view of the imaging system is illustrated in ***Figure. 2A***. The EGI setup, including the ultrasound imaging table, transducer, and rail system, allows precise control during the procedure. The injection stand ensures accurate alignment of the needle with the transducer, which is imperative for a successful injection. Injection micromanipulator screws, located on the injection stand, enable precise movement of the injection clamp holding the syringe in the X-Y plane and control the needle's insertion into the thoracic cavity of the animal. The 3D motor, transducer clamp, transducer mount, animal platform, and micromanipulator screws work together to maintain consistent transducer positioning and enable precise adjustment of the animal table for optimal ultrasound image acquisition. ***Figure. 2B*** represents a close-up view of the rat's positioning during EGI, where the injection clamp can be observed firmly stabilizing the needle during the procedure. ***Figure. 2C*** demonstrates the correct transducer placement relative to the rat, highlighting the alignment of the notch towards the right shoulder to acquire an optimal parasternal long-axis (PSLAX) image. Finally, a frontal view of accurate needle alignment with the transducer is shown in ***Figure. 2D***

The EGI procedure is shown based on B-mode PSLAX images in ***Figure. 3***. First, the 22 G guiding needle was introduced into the thoracic cavity, as shown in ***Figure. 3A*** Then, the 29 G needle was advanced through the guide needle. Upon visualization of the Spinocan® needle, the guide needle was retracted. Then the 29 G needle was advanced into the myocardium (***Fig. 3B***). Consequently, the rCPCs were injected, and the 29 G needle was retracted. The injection was deemed successful upon clear visualization of the injectate (***Fig. 3C***)

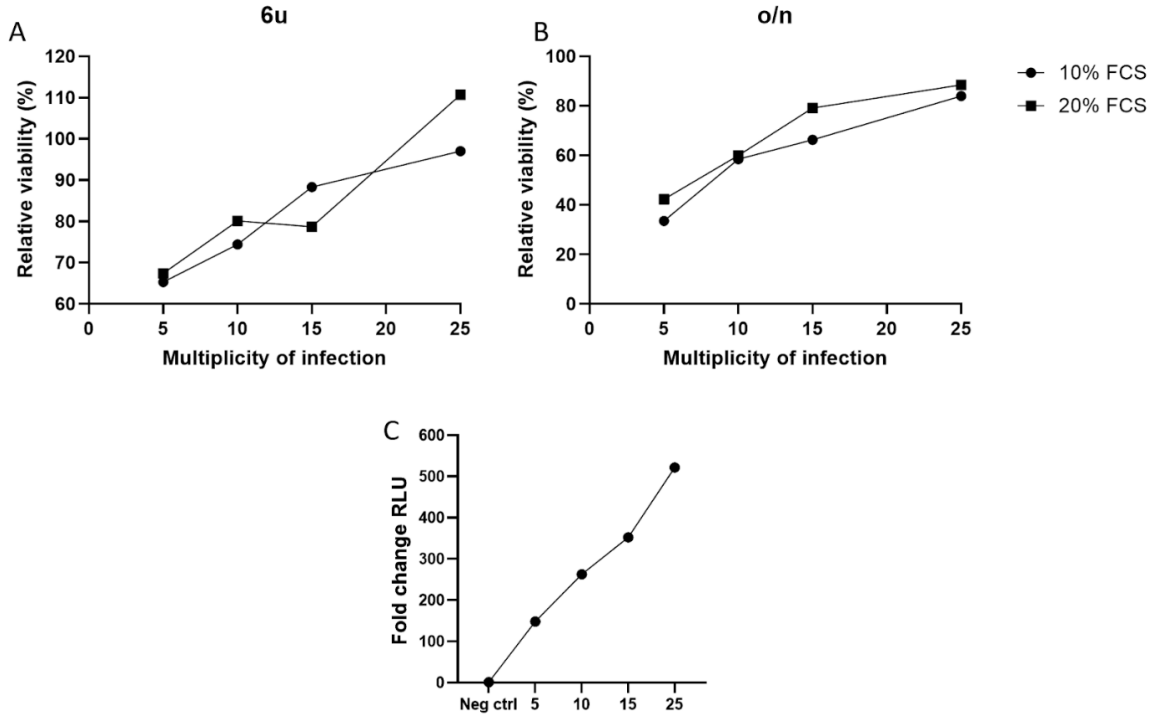

Figure 1. rCPC transduction efficiency and vector expression increase by increasing the multiplicity of infection. – Viability of the rCPCs was assessed using the alamarBlue reagent after puromycin selection following transduction **A**. for 6h, **B**. overnight with increasing MOIs in 10% or 20% FCS. Subsequently, a OneGlo assay confirmed the expression of the introduced vector C. (n = 1). Relative viability was calculated by normalizing the absorbance values to the positive control (i.e., untreated viable cells). Relative light units were calculated by subtracting the background luminescence and creating a fold change relative to the negative control (non-transduced cells). n = 1 for all experiments. RLU, relative light units; o/n, overnight; FCS, fetal calf serum.

EGI safety assessment - Color Doppler imaging was used to assess safety and detect accidental bleeding throughout the EGI procedure. We observed no sign of active bleeding once the 29 G guide needle was advanced into the myocardium (***Fig. 4A***). During the injection, there was no sign of damaging the myocardial integrity to a point of any extra-ventricular blood leakage (***Fig. 4B***). After withdrawal of the needle, no extra-ventricular bleeding in or around the injection site could be observed (***Fig. 4C***). These findings suggest that the left ventricular wall integrity remained intact during and after the EGI procedure, indicating a safe delivery method.

Accurate delivery of Fluc$^+$ rCPCs - rCPCs were transduced using a lentiviral vector to express firefly luciferase to enable *in vivo* tracking of the injectate using BLI. Based on *in vivo* cell tracking, success, efficiency, and accuracy could be determined. ***Figure 5A*** demonstrates partial leakage of the injected cells into the thoracic cavity, attributed to the premature retraction of the needle from the myocardium, as indicated by the presence of a diffuse bioluminescent signal. Conversely, ***Figure 5B*** shows a successful IM delivery of rCPCs, reflected by the intense, centrally localized bioluminescent signal within the left ventricular region. ***Figure 5C*** represents *ex vivo* validation of the precise delivery of rCPCs, demonstrating that the cells were injected specifically into the myocardium. The isolated heart is sectioned into three transverse levels: apex, mid-apex, and mid-ventricular sections. BLI showed the most notable bioluminescent signal in the mid-apex section, confirming a successful, targeted, and efficient IM injection.

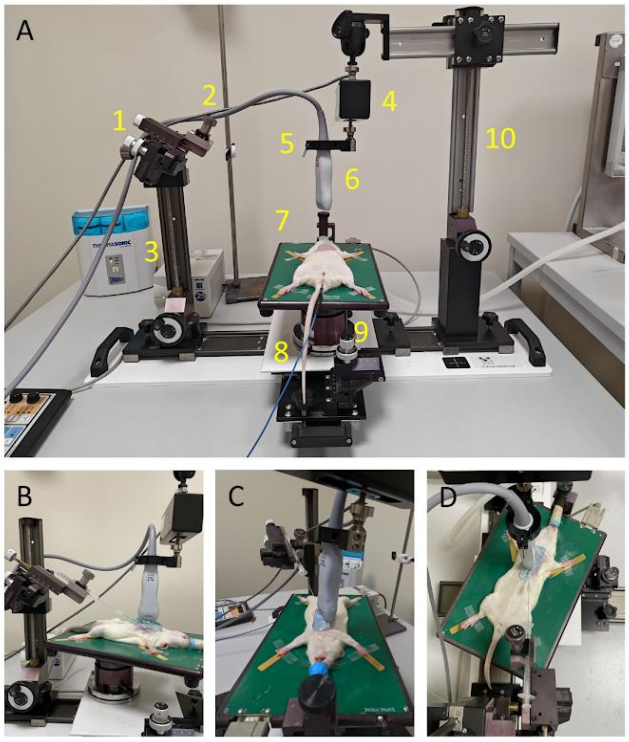

Figure 2. General overview of the EGI setup and animal placement. – **A.** Detailed EGI setup configuration of the ultrasound table, railing system, and injection stand (1. injection micromanipulator screws, 2. injection clamp, 3. injection mount, 4. 3D motor, 5. transducer clamp, 6. transducer, 7. animal platform, 8. animal platform rail, 9. animal platform micromanipulator screws, 10. transducer mount). **B.** EGI close-up and rat positioning. **C.** Positioning of the transducer with the notch aimed at the right shoulder of the rat. **D.** View of the transducer-needle alignment.

Distribution of the injectate through the peri-infarction region - To assess the spatial distribution throughout the injected region, an EGI was executed containing a fluorescent Texas Red Dextran tracer embedded hydrogel matrix. Furthermore, A Sirius Red staining was conducted to visualize the infarcted region. In ***Figure 6A,*** the infarcted region is clearly visible due to the tissue discoloration and thinning, and the injected hydrogel (purple) is positioned in the peri-infarct zone. ***Figure. 6B*** depicts a fluorescent image of a cryosection of the isolated tissue sample counterstained with DAPI for nuclear visualization. The injected tracer can be observed throughout the total thickness of the left ventricular wall, localized in the peri-infarct zone. Nonetheless, exact delivery in the peri-infarct region, where the infarcted tissue is adjacent to the healthy tissue, still remains challenging since echocardiographic identification of the peri-infarcted region relies exclusively on the left ventricular wall thickness. Hence, a Sirius red staining was used to define the localization of the injectate compared to the fibrotic scar of the infarcted region (***Fig. 6C***). These findings reveal that while the injectate was successfully delivered in the border zone of the infarct where there is no left ventricular anterior wall (LVAW) thinning, there is still some fibrosis present at the injection site. This highlights the need for careful selection of the target region for injection.

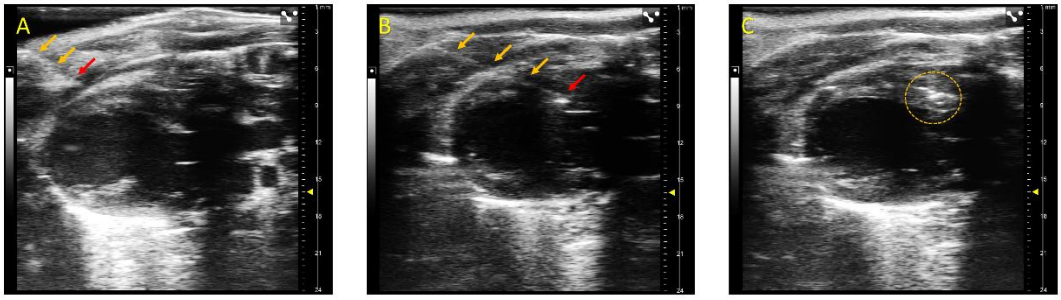

Figure 3. Representative B-mode images of an EGI in PSLAX. – **A. i**nsertion of the 22 G guide needle into the thoracic cavity. **B.** Insertion of the 29 G Spinocan® needle in the left ventricular anterior wall. **C.** Injected rCPCs encircled by the yellow dotted line after the needle withdrawal. Yellow arrows indicate the needle shaft, while red arrows indicate the needle bevel.

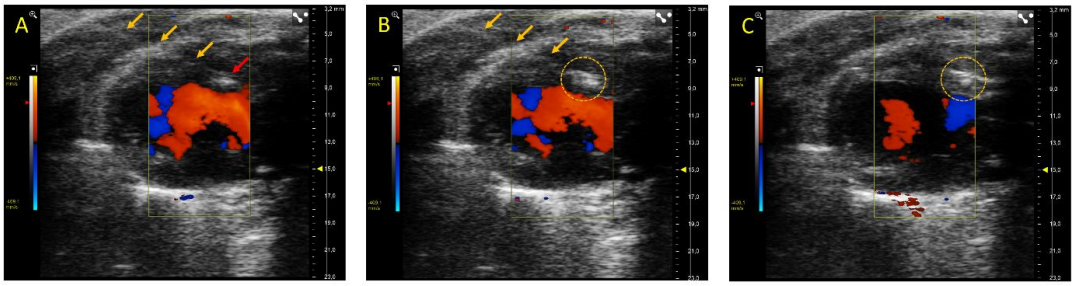

Figure 4. Safety assessment via Doppler imaging of the left-ventricular wall during EGI. – Color Doppler imaging of the left ventricle during the EGI procedure. **A**. Needle insertion phase during the advancement of the 29 G needle in the myocardium. **B**. Injection phase. **C**. Post-injection phase, after needle withdrawal. Yellow arrows indicate the needle shaft, red arrows indicate the needle tip, yellow dotted line delineates the injectate.

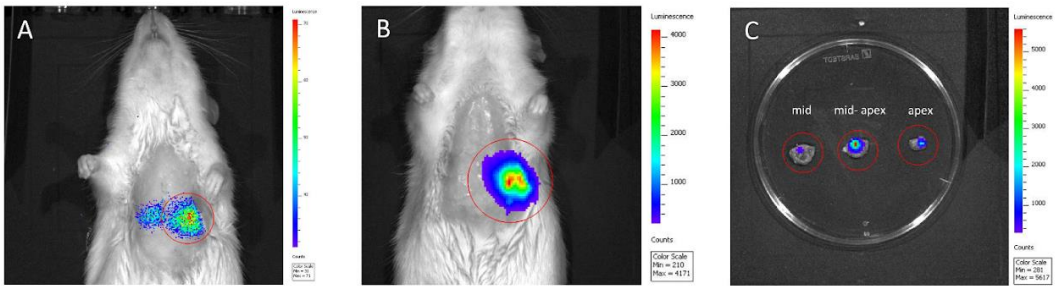

Figure 5. Accuracy and efficiency validation via bioluminescent imaging of the thorax and heart post-EGI. – Fluc^{+} rCPCs were injected using EGI for *in vivo* tracking. **A**. Partial leakage of the injectate into the thoracic cavity after an unsuccessful injection. **B**. Accurate IM injection of rCPCs. **C**. *Ex vivo* imaging of three sections (apex, apex-mid, mid) of the isolated heart. Fluc: firefly luciferase.

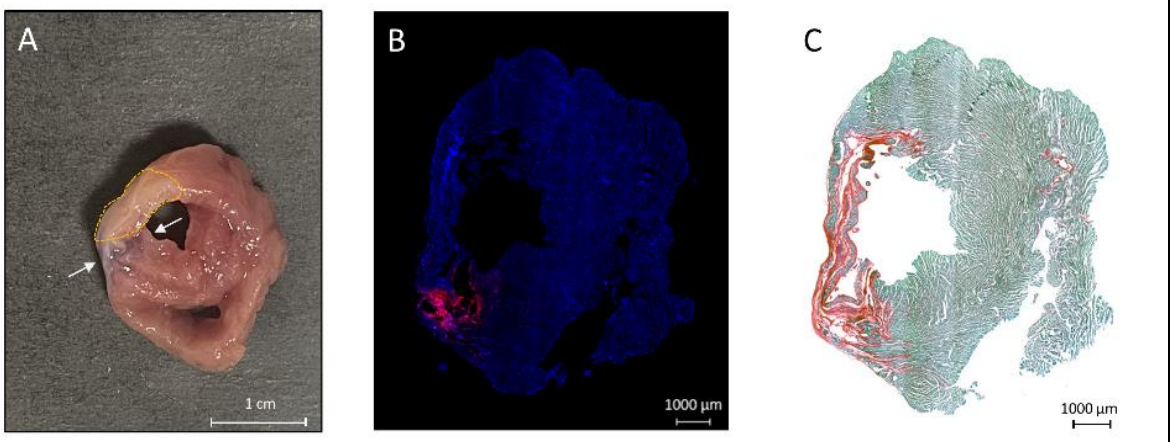

Figure 6. Spatial distribution of the injectate. – A Texas-Red dextran fluorescent tracer embedded in a hydrogel was injected into the peri-infarcted region using EGI. **A**. Section of the heart overviewing the position of the injected hydrogel (between white arrows) relative to the infarcted region (yellow dotted line). **B**. Fluorescent image of a cryosection (10µm) counterstained with DAPI (blue), indicating the Texas-red dextran tracer (red). **C**. Sirius red staining, staining infarcted tissue red and healthy tissue green.

DISCUSSION

In this study, we aimed to develop a refined, innovative approach to deliver therapies intramyocardially using echocardiography-guided injections. We optimized the technique using 29G Spinocan® needles, enabling the injection of rats during PSLAX B-mode imaging, creating a safe and precise injection method.

To enable *in vivo* cell tracking, cells needed to be transduced to produce a bioluminescent signal. Viral transduction is a well-established and effective method to transduce cells, such as primary cells. Furthermore, lentiviral vectors are known to provide more stable gene expression than, for example, adenoviral or adeno-associated viral vectors (19). Transduction efficiency depends on multiple factors, such as the virus type, since some viruses can only infect dividing or non-dividing cells, the origin of the target cell, the adherence of the cell, MOI, and the transduction medium used (19). *Chen et al.* described the superiority of lentiviral vectors over adeno-associated vectors, due to high lentiviral transduction efficiency at a low MOI compared to AAV transduction efficiency at a high MOI (20). With this many variables at play, there is a need for transduction optimization to determine the cell- and virus-specific MOI and transduction conditions. Our rCPC transduction optimization resulted in an optimal MOI of 25 in 20% FCS. Although our results represent a single biological replicate, a clear trend is observed, which allows us to use the findings for subsequent experiments.

Imaging modality and orientation play a critical role in visualizing anatomical landmarks and needle orientation during an EGI. B-mode imaging is the most commonly used modality, as it offers a two-dimensional echocardiographic image capturing all anatomical structures in the plane of the transducer, including the total length of the needle when aligned properly. M-mode relies on the tracing of B-mode images alongside the axis of the plane, creating one-dimensional images. This is ideal for assessing myocardial wall thickness and movement, allowing the operator to identify the injection target site. However, M-mode displays the needle as a single small dot (21). Based on the characteristics of each imaging modality, we conclude that B-mode is the best choice for EGI, since it allows continuous visualization of the needle throughout the thoracic cavity. Besides the imaging mode, the orientation of the image is a critical factor. For instance, imaging could be executed in PSLAX or

SAX. The PSLAX view creates a longitudinal cross-section of the heart, enabling visualization of the total left ventricle, including the apex, the aorta, the papillary muscle, and the base of the heart. The SAX view is obtained by rotating the transducers 90° relative to the PSLAX view, resulting in a transversal cross-section of the heart (21). The most frequently used orientation for EGI is SAX, owing to the anatomical window, accurate targeting of the peri-infarct region, and the relatively short needle trajectory through the thoracic cavity (16, 22, 23). Yet *Prendiville et al.* noted an important difference between injecting in SAX and PSLAX. Specifically, the alignment of the needle with the length of the myocardium allows the needle to be advanced firmly in the muscle, compared to the perpendicular insertion of the needle into the myocardium in SAX imaging (18). Until now, no EGI method using 29 G needles and PSLAX in rats has been described. However, *Tang et al.* performed EGI in SAX using 30 G needles in rats (24). In our experience, however, using a 30 G needle is hardly feasible in rats, due to the short needle length compared to the larger body size of rats (25). Meanwhile, studies using a 28 G needle have been described, but reported off-target delivery of the injectate (26). This can be attributed to the needle bevel size exceeding the thickness of the thinning myocardium after MI (25). Our method addresses these challenges by utilizing an extra-long needle shaft in combination with a fine needle bevel, carefully selected to remain within the LVAW thickness range.

Safety, efficacy, and accuracy are critical components of refining a protocol. We used a hydrogel-embedded Texas-Red dextran tracer in order to visualize the injectate post-injection. As described by *Springer et al.*, the injection of fluorescent tracers is a feasible and reliable technique for post-injection accuracy verification (27). Our results of the Sirius-Red staining and fluorescent imaging are corroborated by the conclusions of *Springer et al.* (27). As evidenced by the localization of the tracer in relation to the infarct zone shown in the Sirius red staining, we were able to execute accurate and robust injections in the peri-infarct zone. However, determination of the peri-infarct zone based on echocardiographic imaging remains challenging, since the only determinant is the LVAW thickness. Nonetheless, this is an extremely important parameter since injection in the infarct zone could result in excessive cell death due to ischemia (17, 28). *Rodriguez-Porcel et al.* described the use of bioluminescent imaging as a method of cell viability after a successful injection over time. They verified that the bioluminescent signal after injection was only emitted by the injected cells, indicating its applicability in MI-induced rat models, therefore justifying the use of BLI to detect the efficiency and accuracy of our injected cells (26). Based on BLI imaging, successful injection of the rCPCs could be observed. Even with an unsuccessful injection, with cell leakage into the thoracic cavity *in vivo*, this scenario could be accurately reflected by BLI. Furthermore, we detected the injected cells *ex vivo* in a heart slice, confirming their retention in the myocardium 24h post-EGI. Although we did not determine the retention of the injected cells multiple days after injection, and the applicability of BLI for longitudinal follow-up, this BLI application was previously described by *Rodriguez-Porcel et al.*, who observed a persistent bioluminescent signal after 24h to 6 days post-injection (26). Similar results were obtained by *Deddens et al.*, who observed a bioluminescent signal 2 days after injection (29). To obtain optimal safety without accidentally puncturing other vital organs, *Nong et al.* determined a thoracic safety window for EGI (16). During our EGI procedure, we adhered to the safety window, additionally, we added color Doppler imaging to assess safety on another level. We observed no intrathoracic or extraventricular bleeding during and after our EGI procedure. Another technique to assess safety is the monitoring of the echocardiogram of the animal for 24h, detecting any arrhythmias caused by the EGI, as described by *Giraldo et al* (30). Another method to detect accuracy and retention is by the use of radioactive hexadecyl-4-[18F]fluorobenzoate labeling to enable detection of the injectate throughout the whole body of the animal using positron emission tomography (31).

Currently, based on clinical and preclinical data, there is no consensus about the most optimal delivery method or for therapeutic agent delivery

in MI models. Given that therapy efficacy can be influenced by the delivery method, the route, or the used stem cells (12, 32). As described earlier, the different methods for clinical delivery are TE, IM, IC, and IV injection. The clinical application of IM injections is less favorable due to their invasive nature (12, 32). While IV is the least invasive method, it lacks retention and implantation in the infarcted region, and cells frequently become trapped in the lungs (12, 32, 33). IC injection is characterized by the direct infusion near the target area, but comes with the risk of embolization, washout, and cannot reach non-perfused areas (17, 32, 34). TE injection is the preferred method, due to its minimal invasiveness, low risk for perforation, and outweighing the risk of a direct IM injection (12, 35). In a pre-clinical setting, invasive IM injection is set as the gold standard over IC or IV approaches, although the same limitations as in clinical settings occur (12, 17, 36). Preclinical studies have proven the great retention capabilities and effectiveness of IM injection over, for example, IC injections. However, the method of a direct IM injection relies on an open-chest procedure, which comes with extreme invasiveness and high risks (36). Hence, minimally invasive procedures, like EGI, are favored over open chest injections because they mimic the clinically applied TE injections, cause less distress for the animal, decrease invasiveness, and are reproducible for multiple injections (16, 24). We optimized this technique to create a standardized and repeatable procedure, to enable longitudinal studies, and to decrease the technical gap in preclinical studies. In these longitudinal studies, it is feasible to repeatedly and accurately target the peri-infarct zone, which is not feasible with open-thorax injections. Moreover, the reduced invasiveness of the procedure increases survival rates. Thereby increasing the translational value of longitudinal preclinical studies and creating consistent preclinical research.

Our technique is susceptible to several limitations. First, the echocardiographic image quality depends on the time point during the different stages of the MI pathology. In the acute phase, extensive tissue damage and adhesion impair qualitative image acquisition. During the chronic phase, the presence of extensive remodeling and severe ventricular wall thinning complicates proper imaging and leaves only limited targetable regions for injection. Furthermore, it is difficult to ascertain the exact infarct extent in real-time, posing the risk of injecting into the infarcted myocardium, which can be detrimental for cell survival. Additionally, infarct variability is a common challenge in rodent models of MI. As a result, a standardized injection site cannot be established and must be individually established for each animal. The technique is limited in injecting all the heart segments, as it only permits access to the anterior, anterolateral, and anteroseptal segments. In order to enable injection in the other segments, ventricular perforation would be necessary.

CONCLUSION

This study presents an optimized, safe, and precise method for IM EGI injection in a rat model of MI. The use of the 29 G Spinocan® needle overcame anatomical differences and enabled precise IM injection, ensuring that the entire injectate remained confined within the myocardium. The methods closely mimic the frequently used clinically relevant TE injection, thereby enabling longitudinal studies involving multiple injections over time. As such, this approach offers a valuable tool to reduce the gap between pre-clinical research and clinical applications.

APPENDIX – Evaluating the safety and efficacy of stem- and root-derived methanolic extracts of *Acacia Karroo in vitro*

INTRODUCTION

In current therapies involving reperfusion of the ischemic area, reperfusion injury (RI) occurs in the cardiac tissue around the ischemic spot. A key characteristic of RI is the overproduction of reactive oxygen species (ROS) due to a chain reaction of metabolic and biochemical changes and cellular stress (5). This excessive production of ROS may compromise the effectiveness of stem cell therapy, as the transplanted cells remain unprotected against ROS despite being embedded in a scaffold designed to improve cell retention. More precisely, these scaffolds do not specifically mitigate oxidative stress that could negatively impact stem cell viability and therapeutic efficacy (37). The excessive production of ROS at the ischemic site in MI adversely impacts the capacity of cells to proliferate, differentiate, modulate the immune response, migrate, and self-renew (38). This highlights the need to develop a strategy that enhances ROS clearance and improves the efficiency of stem cell-driven regenerative therapies to increase their efficacy.

Antioxidant therapy effectively reduces reactive oxygen species (ROS), offering a promising strategy to mitigate oxidative stress and its associated cellular damage. Many trees from the *Acacia* genus have been extensively studied and are known to contain high concentrations of chemicals exhibiting antioxidant capacities (i.e., flavonoids, phenols, and saponins) (39). In particular, the *Acacia Karroo* (*A. Karroo*) species is exceptionally used in native traditional medicine to treat microbial infections and wound healing diseases, and it also exhibits antioxidant and anti-inflammatory effects (40). Phytochemical analysis of *A. Karroo* shows that aqueous-methanolic extracts derived from this plant are rich in epigallocatechin, methyl gallate, quercetin, and flavonoids, which are all antioxidant substances (41). According to More *et al.*, aqueous-methanolic extracts derived from *A. Karroo* showed high free radical scavenging and antioxidant activity based on 2,2-diphenyl-2-picryl-hydraxyl (DPPH) and ferric-reducing antioxidant power assays (41). Based on the abovementioned implications, the *A. Karroo* extract can be an essential therapeutic and prophylactic solution for various diseases, especially in low- to middle-income countries that lack access to modern medicine and where the prevalence of CVD is rising. However, scientific evidence is limited, and the use of *A. Karroo* has never been tested before in a cardiovascular setting, especially in MI, highlighting the need for comprehensive and applicable research. Furthermore, combining the antioxidant extract with regenerative therapy could improve therapeutic efficiency and optimally restore cardiac tissue and its function. Hence, it is necessary first to investigate the safety and efficacy of the methanolic extract of *A. Karroo* derived from different plant parts (i.e., root and stem) on cardiac progenitor and endothelial cells *in vitro*. We hypothesize that the methanolic extract of *A. Karroo* exhibits a beneficial antioxidant effect on cardiac progenitor and endothelial cells via its free radical scavenging capacity, without negatively impacting the survival and proliferation of these cell types.

EXPERIMENTAL PROCEDURES

Animal experiments - Animal regulations were respected as described on page 3. A total of 4 female Sprague-Dawley rats (Janvier Labs, Le Genest-Saint-Isle, France) were utilized in this project.

A. Karroo sample preparation - Stem- and root-derived methanolic extracts of *A. Karroo* were used for several *in vitro* experiments. Regarding the biochemical DPPH assay, *A. Karroo* extract powder was dissolved in a methanol-MilliQ mixture (1:1) to create a stock solution of 10.000µg/mL. For the determination of cytotoxicity and viability, *A. Karroo* extract powder was dissolved in DMSO and was vortexed for several minutes until completely dissolved. Next, culture medium was used to dilute the stock solution to 500 µg/ml (with 1% DMSO). For the *in vitro* cellular assays, the stock solutions of *A. Karroo* were filtered using a 0.2µm sterile syringe filter (Fisher Scientific,

Merelbeke-Melle, Belgium) and serially diluted up to a concentration of 3.90625 µg/mL in culture medium. For the determination of the antioxidant capacity of the extracts, A. Karroo extract powder was again dissolved in DMSO and diluted with culture medium to obtain a stock solution of 50 µg/ml (with 0,1% DMSO).

Cytotoxicity and viability - rCPCs and HUVECs were cultured as described in the Supplementary Methods on page 19. rCPCs were seeded at a density of $27.34x10^3$ cells/cm² in a 96-well plate. HUVECs were seeded at a density of $31.25x10^3$ cells/cm² in a 96-well plate. After adhesion for 24h, cells were either exposed to different concentrations (500, 250, 125, 62.5, 31.25, 15.625, 7.8125, 3.90625 µg/mL) of stem- or root-derived extract of *A. Karroo*, or to corresponding concentrations of DMSO. Cell viability was assessed using the alamarBlue™ protocol as described on page 3. Cells cultured with PBS were used as the negative control, and culture with enriched medium were used as the positive control. Experiments were executed in triplicate. The percentage of alamarBlue reduction was calculated according to the manufacturer's guidelines, and subsequently normalized to the negative control for cytotoxicity and positive control for viability.

ROS assay - rCPCs and HUVECs were cultured as described in the Supplementary Methods on page 19. A 2',7'-dichlorofluorescein (DCF) assay was performed to assess the antioxidant effect of the stem- and root-derived methanolic extracts of *A. Karroo*. Cells were seeded at 6250 cells/cm². First, cells were exposed for 3h to phorbol-12-myristate-13-acetate (PMA) (100 ng/mL) (Sigma-Aldrich, Hoeilaart, Belgium). Subsequently, cells were treated with decreasing concentrations of root- and stem-derived extracts (50, 25,12.5, 6.25, 3.125 µg/mL) for 24h. After exposure, cells were incubated for 45 min with 10µM DCFDA probe (Sigma-Aldrich, Hoeilaart, Belgium) and washed using PBS. Fluorescence was obtained (excitation: 494nm/ emission: 522nm) using a microplate reader (Clariostar Plus, BMG Labtech, Ortenberg, Germany). Next, the cells were fixated with 50 µl Trichloroacetic acid-Sulforhodamine B (TCA-SRB) (0.004% w/v SRB in 10% w/v TCA) (Sigma-Aldrich, Hoeilaart, Belgium) for 15 min, and washed with 1% acetic acid afterwards. Ultimately, cells were incubated with 10 mM Trizma base (Sigma-Aldrich, Hoeilaart, Belgium) for 5 min at room temperature. Fluorescence was acquired (ex: 565 nm/ em: 586 nm) using a microplate reader (Clariostar Plus, BMG Labtech, Ortenberg, Germany).

Statistical analysis - Statistical analysis was performed using GraphPad Prism (GraphPad Software, version 10.4.1 (627)). Outliers were identified and excluded using the Rout test (Q=10%), and normality was assessed with the Shapiro-Wilk test. Non-linear regression was performed to compare the IC_{50} and CC_{50} values of the different extracts relative to the vehicle control. A two-way ANOVA was executed to determine differences in concentrations in the cytotoxicity assay. For experiments performed at different time points, a one-way ANOVA, followed by a Tukey multiple comparison, was performed for normally distributed data, and a non-parametric Kruskal-Wallis test, followed by a Dunn's multiple comparison, was used for non-normally distributed data at a specific time point. All data are expressed as mean ± standard deviation (SD), $p < 0.05$ is considered statistically significant.

RESULTS

Filter sterilization reduces the free radical scavenging capacity of the methanolic stem-derived extract of A. Karroo - A DPPH assay, as described in the supplementary materials on page 19 was performed on both the stem- and root-derived methanolic extracts of *A. Karroo* to determine the effect of filter sterilization on their free radical scavenging capacity. No significant differences were observed between the $logIC_{50}$ values of the filtered and unfiltered root extract ***(Fig. S1A, Table S1;*** *0.9258 for filtered root extract, 0.8686 for unfiltered root extract, p = 0.0863)*. Translating these $logIC_{50}$ values to a concentration, the IC_{50} of the filtered root extract was 8.430 µg/ml, compared to the IC_{50} of the unfiltered root extract being 7.390 µg/ml. This suggests a small, insignificant reduction in free radical scavenging capacity. However, a

significant difference was detected between the $logIC_{50}$ values of the filtered and unfiltered stem extracts (***Fig. S1B***; 0.9237 *for filtered stem extract, 0.7368 for unfiltered stem extract,* $p < 0.001$). These $logIC_{50}$ values respectively represent an IC_{50} of 8.388 µg/ml and 5,455 µg/ml, indicating a reduction in free radical scavenging capacity after filtration of the stem-derived methanolic extract of *A. Karroo*.

High concentrations of both root- and stem-derived methanolic extracts of A. Karroo tends to exert cytotoxic effects - To determine whether the methanolic extracts of *A. Karroo* have a cytotoxic effect on various cell types. HUVECs and rCPCs were exposed to increasing concentrations of stem- and root-derived extracts, or to corresponding concentrations of DMSO as a vehicle control, for 24h. In relation to the HUVECs, 500 µg/ml of the stem- and root-derived extract of *A. Karroo* is significantly more cytotoxic compared to the vehicle control (i.e. 1% DMSO) (***Fig. 1A****; stem 94.408% ± 5.954%; root 68.563% ± 37.159% vs. DMSO 8.020% ± 21.752%, p<0.0001; p<0.01*). Regarding the half-maximal cytotoxic concentration (CC_{50}), HUVECs exhibit a $logCC_{50}$ of 2.488 after stem-derived extract treatment and a $logCC_{50}$ of 2.431 after root-derived treatment, respectively, a CC_{50} of 307.5 µg/mL and 269.6 µg/mL. No significant difference in CC_{50} is observed. In relation to the rCPCs, no significant differences in cytotoxic effects were observed for increasing concentrations of the extracts compared to DMSO. rCPCs exhibit a $logCC_{50}$ of 0.2666 after stem-derived extract treatment and a $logCC_{50}$ of 0.09232 after root-derived treatment (***Fig. 1B***). Nonetheless, a similar dose-dependent trend can be observed in the rCPCs as observed in the HUVECs.

Chronic exposure to increasing concentrations of stem- and root-derived extracts of A. Karroo does not critically impair the viability of HUVECs and rCPCs - To assess whether chronic exposure to *A. Karroo* affects the viability of HUVECs and rCPCs, these cells were exposed to increasing concentrations of stem- and root-derived methanolic extracts for 24h, 48h, and 72h. After 24h and 48h, HUVECs showed a significant decrease in viability after treatment with 500 µg/mL of the root-derived extract of *A. Karroo,* compared to the vehicle control, respectively, (***Fig. 1C****; 31.44% ± 37.16% vs 91.98% ± 21.75%, p = 0.0299 at 24h, 22.55% ± 27.44% vs 77.05% ± 9.147%, p = 0.001 at 48h*). However, after 72 hours of exposure, no significant differences were observed. Regarding the stem-derived extract of *A. Karroo*, a significant difference could be observed between 500 µg/mL treatment and the vehicle control group after 24h and 72h, respectively (***Fig. 1D****, 5.593% ± 5.954% vs 91.98% ± 21.75%, p = 0.0025 at 24h, and -2.885% ± 2.320% vs 142.1% ± 55.71%, p = 0.0447 at 72h*). Although exposure to 500 µg/mL of stem- and root-derived extract has drastically reduced cell viability, no additional significant differences were observed. The same trend can be observed for the viability in rCPCs after chronic treatment with increasing concentrations of both extracts; however, it is still insignificant due to a low sample size (***Fig. 1E-F***).

ROS reduction - In order to test the antioxidant capacity of *A. Karroo*, ROS was induced using PMA. Afterwards, cells were treated with increasing concentrations of the root- and stem-derived *A. Karroo* extracts. However, no significant results were observed in HUVECs after treatment with the stem- and root-derived extract (***Fig. 3A-B***). Additionally, evaluation of relative ROS levels in rCPCs depicted no significant reduction in relative ROS levels after treatment with the increasing concentrations of stem- and root-derived extracts of *A. Karroo* (***Fig. 3C-D***). In general, the relative ROS levels of the untreated cells are comparable to those that have been exposed to PMA.

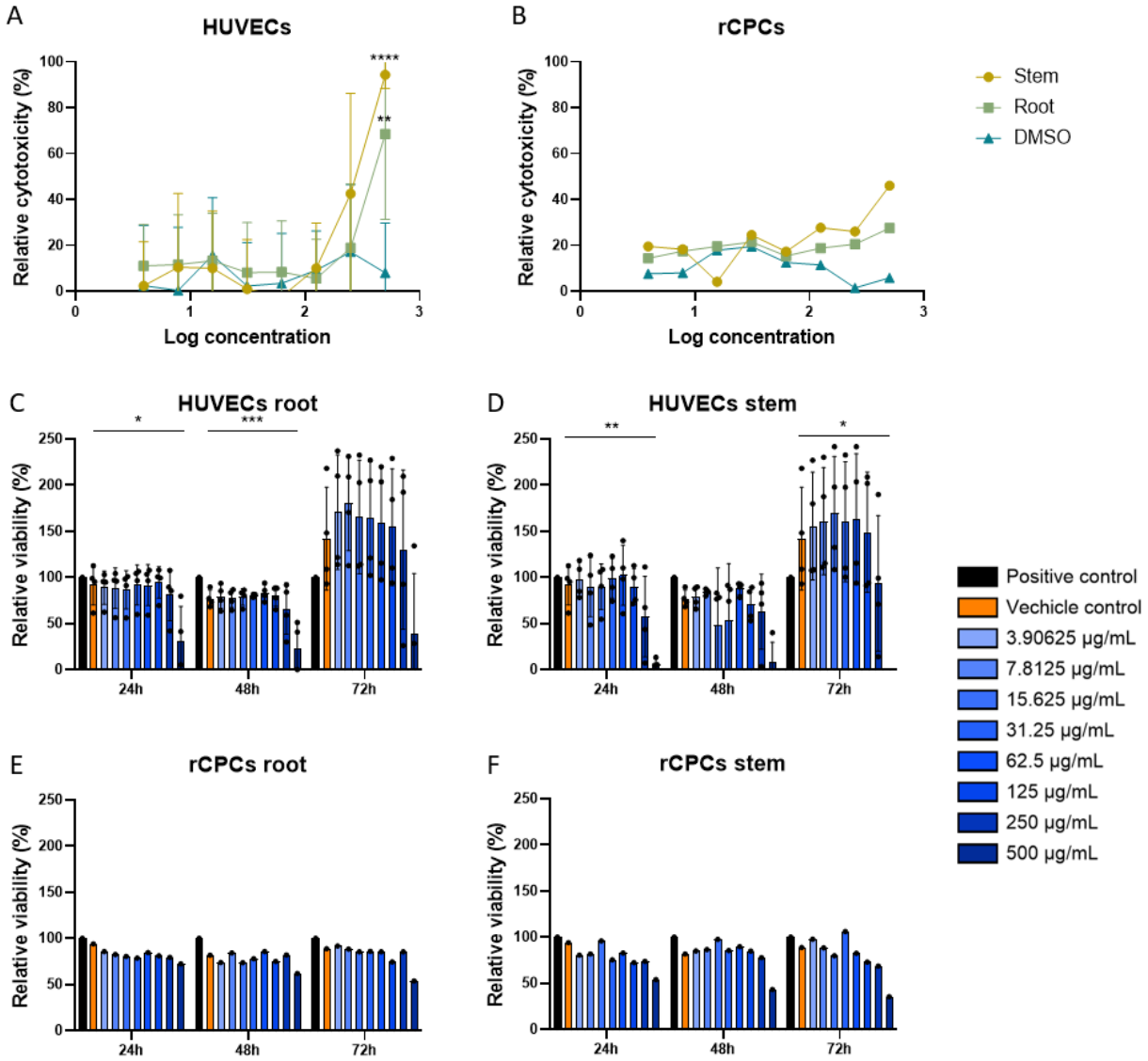

Figure 1. High concentrations of stem- and root-derived extracts tend to have cytotoxic effects without critically affecting the viability after chronic exposure in HUVECs and rCPCs. – (**A**) Cytotoxicity on HUVECs (n = 4) (**B**) and rCPCs (n = 1) was assessed with alamarBlue reagent after 24h of treatment with either stem- or root-derived extracts of A. Karroo or corresponding concentrations of DMSO as a vehicle control. Experiments were performed in triplicate, and the percentage of cytotoxicity was calculated using the absorbance values. Data were normalized against the viability of the negative control (i.e., no viable cells). (**C-D)** Cell viability of HUVECs (n = 4), (**E-F)** and rCPCs (n = 1) was assessed using alamarBlue reagent after exposure to increasing concentrations of stem- and root-derived extracts of A. Karroo or to corresponding concentrations of DMSO as a vehicle control, for either 24h, 48h, or 72h. Experiments were performed in triplicate, and percentages of viability were calculated using the absorbance values. Data were normalized against the positive control (i.e., untreated viable cells) to calculate the percentage of relative viability. Data is represented as the mean ± SD. * p denotes < 0.5, ** denotes $p < 0.01$, *** denotes $p < 0.001$, **** denotes $p < 0.0001$. DMSO, dimethylsulfoxide; HUVECs, human umbilical vein endothelial cells; rCPCs, rat cardiac progenitor cells.

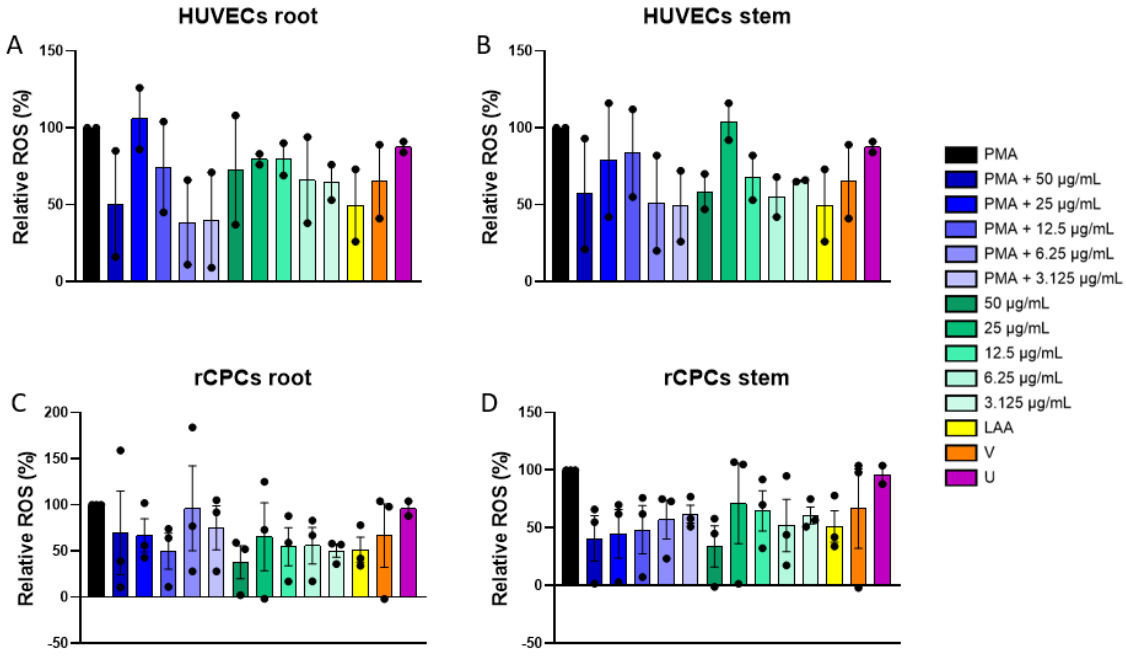

Figure 2. Increasing concentrations of root- and stem-derived methanolic extracts of A. Karroo do not reduce PMA-induced ROS levels. – (**A-B**) ROS was induced by exposing HUVECs (n = 2) (**C-D**) and rCPCs (n = 3) to PMA (100 ng/mL) for 3h, after which they were treated with increasing concentrations of root- and stem-derived A. Karroo extracts for 24h. The fluorescent, DCFDA (10µM) probe was used to detect ROS levels. TCA-SRB was used to correct for cell count. Experiments were performed in triplicate, and the percentage of relative ROS levels was calculated using the fluorescence values. Data were normalized against the untreated control (i.e., no PMA, no extract), the DCFDA: TCA-SRB was normalized against the mean PMA to obtain the relative ROS levels. Data were represented as the mean ± SD. ROS, reactive oxygen species; PMA, phorbol 12-myristate 13-acetate; HUVECs, human umbilical vein endothelial cells; rCPCs, rat cardiac progenitor cells; DFCDA, 2',7'-dichlorofluorescein diacetate; TCA, trichloroacetic acid; SRB, sulforhodamine B.

DISCUSSION

The aim of this study was to determine the safety and efficacy of methanolic stem- and root-derived extracts of *A. Karroo*. The effect of the extracts was determined based on cytotoxicity, viability, and ROS reduction in both HUVECs and rCPCs. Due to technical limitations, we were unable to determine their effect on proliferation. Another limitation is the small sample size, due to the scarcity of cells and constraints on time.

In order to do *in vitro* experiments with the extracts, the effect of filter sterilization on the potency of the extracts had to be assessed. The DPPH assay revealed a significant reduction in the IC_{50} of the stem-derived extract, from 8.388 µg/ml for unfiltered extract to 5.455 µg/ml after filtration. This may imply that some antioxidant biochemical compounds present in the extract are filtered out. Taking this into account, a higher concentration of filtered stem-derived extract may be necessary to achieve equivalent effects to those obtained with unfiltered extract. Unlike the stem-derived extract, filtration of the root-derived extract did not change the IC_{50} significantly, suggesting little to no loss of antioxidant compounds after filtration and possibly reflecting a different distribution of antioxidant compounds across various parts of the *A. Karroo*. Similar observations have been reported by *Abdel-Farid et al*., as they observed a divergent distribution of flavonoids, phenolics, saponins, and proteins

throughout the leaves and the flowers of *A. nilotica*, *A. seyal*, and *A. laeta* (39). However, phytochemical analysis using nuclear magnetic resonance or ultra-high-performance liquid chromatography–quadrupole time-of-flight mass spectrometry analysis, as described by *More et al.*, should be executed to determine the biochemical profile of the stem- and root-derived methanolic extracts of *A. Karroo*, before and after filter sterilization *(41)*.

Cytotoxicity and viability were assessed to determine the effect of acute and chronic exposure to stem- and root-derived extracts of A. Karroo. Exposure for 24h with the stem- and root-derived extracts at a concentration of 500 µg/mL showed a significant increase in cytotoxicity in HUVECs, compared to the vehicle control, confirming that high concentrations of both extracts exert cytotoxic effects. Furthermore, *Njanje et al.* determined the CC_{50} of an acetonic *A. Karroo* leaf-derived extract ranging from 490 µg/mL to 570 µg/mL in muscle cells, and from 310 µg/mL to 330 µg/mL in adipose cells, based on the type of preparation of the extract (i.e., non-defatted vs. defatted extracts) (42). Furthermore, *Tshikalange et al.* determined a CC_{50} of 115 µg/mL based on the ethanolic extract in Vero African monkey cells (43). The results indicated that the CC_{50} may be dependent on the cell type and preparation of the extract. When considered alongside the DPPH data, these findings suggest a potentially safe and therapeutic window between 10 µg/mL and 100 µg/mL for *in vitro* experiments.

Previously mentioned findings on the cytotoxicity of stem- and root-based extracts of *A. Karroo* are in line with the results of the viability, as a significant reduction in HUVECs viability was observed only after 24 and 48 hours of exposure to 500 µg/mL of the root-derived extract, and after 24 and 72 hours of exposure to 500 µg/mL of the stem-derived extract. Although time-dependent effects were not statistically evaluated, the similar viability levels observed at 24, 48, and 72h for each concentration suggest that prolonged exposure does not further reduce cell viability. This observation indicates that the concentration of the extracts may be the primary factor influencing cell viability under these conditions. Similar results have been reported by *Chiaino et al.*, who noticed a significant decrease in the viability of HT-29 cells after exposure to 250 µg/mL and 500 µg/mL of *A. Catechu* after 24, 48, and 72h, suggesting that reduced viability is mainly driven by concentration rather than treatment duration (44). Considering these extracts may eventually be used as dietary supplements, once approved for safety and efficacy and an optimal dose has been determined, these data may suggest that chronic intake of these extracts does not drastically impact cell viability. Nonetheless, as described by *Adedapo et al.*, *in vivo* exposure to at least 1600 mg/kg of aqueous *A. Karroo* extract for 16h resulted in mortality after 48h in mice (45). This highlights the need for further *in vitro* experimentation and validation. Additionally, pharmacokinetic principles and cumulative doses have to be taken into account when translating *in vitro* concentrations to *in vivo* doses.

Once the safety of the stem- and root-derived extracts were established, their antioxidant potential was subsequently examined. However, as relative ROS levels did not significantly differ between the positive control (i.e., PMA only) and the vehicle control (i.e., 0.1% DMSO) or the untreated control, our data indicate that ROS induction failed, as ROS levels after PMA induction were not significantly increased compared to the untreated control. Normally, PMA binds to and subsequently activates protein kinase C (PKC). Hereby, an overactivation of NADPH oxidase (NOX) occurs, drastically increasing ROS production (46). However, it is important to note that the binding of PMA to PKC is reversible, furthermore, PMA is photosensitive and sensitive to freeze-thaw cycles (47). The absence of ROS production following PMA in our assay may be attributed to differences in experimental design compared to other published protocols (46). Specifically, while similar concentrations of PMA and DCFDA were used, the timing and order of reagent application differed. In contrast to our approach, where ROS was first induced with PMA for 3h, followed by antioxidant treatment of 24h and subsequent DCFDA loading, *Ponath et al.* loaded cells with DCFDA prior to immediate ROS induction with PMA for 30 min (46). Furthermore, they detected

ROS via flow cytometry, whereas a plate reader was used in our setup. Given the reversible nature of PMA binding to PKC, these methodological differences may have prevented successful ROS induction in our assay. Interestingly, *Behnen et al.* discovered that PMA-related ROS induction is dependent on the extracellular acidic pH (48). More precisely, an acidic extracellular environment caused a reduced efficiency of ROS production. Although lowering the extracellular pH led to a reduction in ROS production, the levels remained substantially higher than those of the untreated control (48). In general, the results derived from our experiment should be interpreted with caution, suggesting the urgent need for PMA optimization before any further experimentation.

While this study provides compelling evidence that cytotoxic effects of stem- and root-derived extracts from *A. Karroo* are more likely concentration-dependent than time-dependent. It is necessary to execute extensive research, adhering to the ADME (absorption, distribution, metabolization, and excretion) principles in order to enable *in vivo* testing. Despite the effort, ROS induction using PMA should be optimized, and the experimental setup should be adapted according to the optimization. As a future perspective, this study could be repeated using induced pluripotent stem cell-derived cardiomyocytes; this way, it is possible to determine the effect on contractility and physiology.

CONCLUSION

In general, we can conclude that filter sterilization of stem-derived extracts of *A. Karroo* may result in a reduced antioxidant activity, which needs to be taken into account for future *in vitro* experiments. Based on our data, a potentially safe therapeutic window between 10 µg/mL and 100 µg/mL can be applied and used for further analysis, as extensive *in vitro* safety and ROS reduction testing needs to be executed before any further *in vivo* application of the extract can even be considered.

Acknowledgements – I would like to express my heartfelt gratitude to Ellen and Lotte for their exceptional guidance throughout this project. Your support and expertise have been invaluable to me. A special thanks to Ellen for making the long days in the animalium not only bearable but genuinely enjoyable. Your positive attitude and encouragement created a working atmosphere that made even the most challenging moments worthwhile. Lotte, I am truly grateful for your dedication and commitment. Even though the project faced some setbacks, you went above and beyond to help bring this thesis to a strong and meaningful end. Lastly, I would like to sincerely thank Prof. dr. Bito for promoting this research and providing the opportunities along the way. Your trust and belief in this work have played a vital role in making this all possible. Thank you all!

Author contributions – Writing of the thesis is executed by Vincent Vandenboer. Feedback on the thesis was provided by Ellen and Lotte. Experimental procedures were executed under the guidance and supervision of Ellen and Lotte.

SUPPLEMENTARY MATERIALS AND METHODS

Myocardial infarction induction - Rats were anesthetized using 5% isoflurane supplemented with oxygen at a flow rate of 2 L/min. Subsequently, rats were intubated orotracheally and mechanically ventilated using the Inspira ASV ventilator (Harvard Apparatus, Massachusetts, United States) and received prophylactic buprenorphine 0.04 mg/kg (Richter Pharma AG, Wels, Austria). A left thoracotomy was performed within the 3rd intercostal space to expose the heart. The pericardium was opened, and the left anterior descending coronary artery (LAD) was ligated using an 8/0 Prolene suture (Ethicon, Deforce Medical, Ardooie, Belgium). Successful MI induction was visually verified through immediate pallor of the left ventricle post-ligation. Exclusively, animals showing apparent left ventricle pallor were included in the study (n=19). The chest and skin were closed using 5/0 Vicryl rapide (Ethicon, Deforce Medical, Ardooie, Belgium). When spontaneous respiration returned, the animal was extubated.

rCPCs isolation and cell culture - rCPCs were isolated from the right atrial appendage (RAA) of rats. Briefly, rats were injected with heparin (Leo Pharma Nv, Lier, Belgium) (1000 units/kg intraperitoneally (i.p.)) and subsequently sacrificed with an overdose of sodium pentobarbital (Dolethal, Vetoquinol, Aartselaar, Belgium, 200 mg/kg, i.p.). Hearts were harvested, perfused using a standard phosphate-buffered saline (PBS) solution, and the RAAs were collected. The extracted RAA tissue was minced into pieces of ± 1 mm^3, subsequently washed with PBS, and enzymatically dissociated using Hank's Balanced Salt Solution (HBSS) (Lonza, Basel, Switzerland) supplemented with 0,6 WU/ml collagenase NB4 (Serva, Heidelberg, Germany) and 300 mM $CaCl_2$. Using the Aldefluor Assay kit (StemCell Technologies, Evergem, Belgium), the rCPCs were stained according to the manufacturer's protocol and flow-sorted using the FACS Aria (BD Biosciences, Erembodegem, Belgium) in X-Vivo 15 medium (Lonza, Basel, Switzerland) supplemented with 20% fetal calf serum (FCS) and 2% penicillin/ streptomycin (P/S), further referred to as enriched medium. Sorted rCPCs were seeded in a six-well plate and incubated at 5% CO_2 at 37°C. rCPCs were maintained using enriched X-vivo medium and passaged upon reaching 80-90% confluence.

HUVEC expansion - HUVECs from pooled donors (Lonza, Basel, Switzerland) were cultured using EGM®-2 Endothelial Cell Growth Medium-2 BulletKit® (Lonza, Basel, Switzerland), incubated at 37°C in a 5% CO_2 atmosphere. HUVECs were passaged using trypsin at 80-90% confluence and seeded in a T75 culture flask at a density of 24 000 cells/ cm^2. Cells were frozen in cryovials of 500.000 cells/mL in EGM-2 medium (Lonza, Basel, Switzerland) supplemented with 10% dimethylsulfoxide (DMSO).

Hydrogel preparation - The ELR hydrogel consisted of HE5 cyclooctyne (128.56 mg/mL) and HRGD6 azide (35.7 mg/mL) components (Bioforge, Valladolid University), respectively, components A and B. Solid hydrogel components were weighed and dissolved in basal X-Vivo medium and incubated on ice at 4°C overnight. The hydrogel was formulated at the following ratios: 25% rCPCs suspended in basal X-Vivo medium, 25% component A, and 50% component B.

DPPH assay - To determine the effect of filter sterilization of the extract solution, the DPPH free radical scavenging assay described by *More et al.* (2021), was performed with a slight modification of the protocol (41). First, the extract was filtered using a Millex-GV PVDF syringe filter (0,22µm, 4mm) (Millipore, Merck, Darmstadt, Germany). Then, 20µL of 10.000 µg/mL extract was diluted with 180µL methanol in the top row of a 96-well plate. A serial dilution was established in the remaining wells of the 96-well plate. Finally, 100µL of DPPH solution (625µM) was added and incubated for 30 minutes at room temperature. After adding DPPH, the final concentrations (in µg/mL) of the extract were: 500, 250, 125, 62.5, 31.25, 15.625, 7.8125, and 3.90625, respectively. L-ascorbic acid (1 mM) was used as the positive control, DPPH solution (625µM) as the negative control, and methanol-MilliQ (1:1) as the vehicle control. Absorbance was measured using a microplate reader (Clariostar Plus, BMG Labtech,

Ortenberg, Germany) at 517nm. This experiment was performed in five replicates. To calculate the percentage of free radical scavenging, the following formula was used: DPPH radical scavenging effect (%) = $\left(\frac{A0-At}{A0}\right) x\ 100$ where A_0 is the absorbance blank, and A_t is the absorbance tested sample.

SUPPLEMENTARY RESULTS

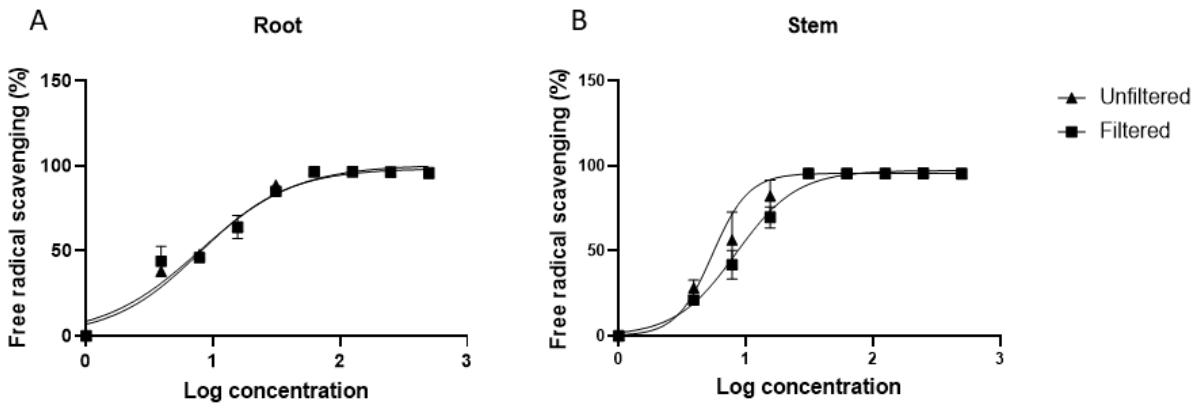

Figure S1. Effect of filter sterilization on the free radical scavenging capacity of stem- and root-derived methanolic extracts of A. Karroo. – Via the DPPH assay, the IC_{50} values of both unfiltered and filtered extracts of (**A**) the root and (**B**) the stem were obtained. This experiment was performed in quintuplicate. Curves were fit via nonlinear regression. Data points represent mean ± SD. ** denotes $p < 0.01$, *** denotes $p < 0.001$. IC_{50}, half-maximal inhibitory concentration.

Table S1. Effect of filter sterilization on the free radical scavenging activity of stem- and root-derived methanolic extracts of A. Karroo.

Extract	Filtered	Unfiltered
Root	0.9258	0.8686
Stem	0.9237***	0.7368

Antioxidant activity was determined using the DPPH assay of both unfiltered and filtered extracts of the root and the stem. The experiment was performed in quintuplicate. $LogIC_{50}$ were obtained via nonlinear regression. Data represents mean ± SD. *** denotes $p < 0.001$. IC_{50}, half-maximal inhibitory concentration.

REFERENCES

1. Martin SS, Aday AW, Almarzooq ZI, Anderson CAM, Arora P, Avery CL, et al. 2024 Heart Disease and Stroke Statistics: A Report of US and Global Data From the American Heart Association. Circulation. 2024;149(8):e347-e913.
2. organisation WH. Cardiovascular diseases (CVDs) 2021 [Available from: https://www.who.int/news-room/fact-sheets/detail/cardiovascular-diseases-(cvds).
3. Jenca D, Melenovsky V, Stehlik J, Stanek V, Kettner J, Kautzner J, et al. Heart failure after myocardial infarction: incidence and predictors. ESC Heart Fail. 2021;8(1):222-37.

4. Berezin AE, Berezin AA. Adverse Cardiac Remodelling after Acute Myocardial Infarction: Old and New Biomarkers. Dis Markers. 2020;2020:1215802.
5. Wu MY, Yiang GT, Liao WT, Tsai AP, Cheng YL, Cheng PW, et al. Current Mechanistic Concepts in Ischemia and Reperfusion Injury. Cell Physiol Biochem. 2018;46(4):1650-67.
6. Saito Y, Oyama K, Tsujita K, Yasuda S, Kobayashi Y. Treatment strategies of acute myocardial infarction: updates on revascularization, pharmacological therapy, and beyond. J Cardiol. 2023;81(2):168-78.
7. Yamada Y, Minatoguchi S, Kanamori H, Mikami A, Okura H, Dezawa M, et al. Stem cell therapy for acute myocardial infarction - focusing on the comparison between Muse cells and mesenchymal stem cells. J Cardiol. 2022;80(1):80-7.
8. Scimia MC, Gumpert AM, Koch WJ. Cardiovascular gene therapy for myocardial infarction. Expert Opin Biol Ther. 2014;14(2):183-95.
9. Beeri R, Chaput M, Guerrero JL, Kawase Y, Yosefy C, Abedat S, et al. Gene delivery of sarcoplasmic reticulum calcium ATPase inhibits ventricular remodeling in ischemic mitral regurgitation. Circ Heart Fail. 2010;3(5):627-34.
10. Jayawardena TM, Egemnazarov B, Finch EA, Zhang L, Payne JA, Pandya K, et al. MicroRNA-mediated in vitro and in vivo direct reprogramming of cardiac fibroblasts to cardiomyocytes. Circ Res. 2012;110(11):1465-73.
11. Khalili MR, Ahmadloo S, Mousavi SA, Joghataei MT, Brouki Milan P, Naderi Gharahgheshlagh S, et al. Navigating mesenchymal stem cells doses and delivery routes in heart disease trials: A comprehensive overview. Regen Ther. 2025;29:117-27.
12. Kanelidis AJ, Premer C, Lopez J, Balkan W, Hare JM. Route of Delivery Modulates the Efficacy of Mesenchymal Stem Cell Therapy for Myocardial Infarction: A Meta-Analysis of Preclinical Studies and Clinical Trials. Circ Res. 2017;120(7):1139-50.
13. Liew LC, Ho BX, Soh BS. Mending a broken heart: current strategies and limitations of cell-based therapy. Stem Cell Res Ther. 2020;11(1):138.
14. Rodrigo SF, van Ramshorst J, Hoogslag GE, Boden H, Velders MA, Cannegieter SC, et al. Intramyocardial injection of autologous bone marrow-derived ex vivo expanded mesenchymal stem cells in acute myocardial infarction patients is feasible and safe up to 5 years of follow-up. J Cardiovasc Transl Res. 2013;6(5):816-25.
15. Jia T, Wang C, Han Z, Wang X, Ding M, Wang Q. Experimental Rodent Models of Cardiovascular Diseases. Front Cardiovasc Med. 2020;7:588075.
16. Nong Y, Guo Y, Tomlin A, Zhu X, Wysoczynski M, Li Q, et al. Echocardiography-guided percutaneous left ventricular intracavitary injection as a cell delivery approach in infarcted mice. Mol Cell Biochem. 2021;476(5):2135-48.
17. Li J, Hu S, Zhu D, Huang K, Mei X, Lopez de Juan Abad B, et al. All Roads Lead to Rome (the Heart): Cell Retention and Outcomes From Various Delivery Routes of Cell Therapy Products to the Heart. J Am Heart Assoc. 2021;10(8):e020402.
18. Prendiville TW, Ma Q, Lin Z, Zhou P, He A, Pu WT. Ultrasound-guided transthoracic intramyocardial injection in mice. J Vis Exp. 2014(90):e51566.
19. Chong ZX, Yeap SK, Ho WY. Transfection types, methods and strategies: a technical review. PeerJ. 2021;9:e11165.
20. Chen C, Akerstrom V, Baus J, Lan MS, Breslin MB. Comparative analysis of the transduction efficiency of five adeno associated virus serotypes and VSV-G pseudotype lentiviral vector in lung cancer cells. Virol J. 2013;10:86.

21. Silva J, Azevedo T, Ginja M, Oliveira PA, Duarte JA, Faustino-Rocha AI. Realistic Aspects of Cardiac Ultrasound in Rats: Practical Tips for Improved Examination. J Imaging. 2024;10(9).
22. Ghanem A, Ziomka A, Krausgrill B, Schenk K, Troatz C, Miszalski-Jamka T, et al. Functional impact of targeted closed-chest transplantation of bone marrow cells in rats with acute myocardial ischemia/reperfusion injury. Cell Transplant. 2009;18(12):1289-97.
23. Follin B, Hoeeg C, Hojgaard LD, Juhl M, Lund KB, Dossing KBV, et al. The Initial Cardiac Tissue Response to Cryopreserved Allogeneic Adipose Tissue-Derived Mesenchymal Stromal Cells in Rats with Chronic Ischemic Cardiomyopathy. Int J Mol Sci. 2021;22(21).
24. Tang XL, Nakamura S, Li Q, Wysoczynski M, Gumpert AM, Wu WJ, et al. Repeated Administrations of Cardiac Progenitor Cells Are Superior to a Single Administration of an Equivalent Cumulative Dose. J Am Heart Assoc. 2018;7(4).
25. Zacchigna S, Paldino A, Falcao-Pires I, Daskalopoulos EP, Dal Ferro M, Vodret S, et al. Towards standardization of echocardiography for the evaluation of left ventricular function in adult rodents: a position paper of the ESC Working Group on Myocardial Function. Cardiovasc Res. 2021;117(1):43-59.
26. Rodriguez-Porcel M, Gheysens O, Chen IY, Wu JC, Gambhir SS. Image-guided cardiac cell delivery using high-resolution small-animal ultrasound. Mol Ther. 2005;12(6):1142-7.
27. Springer ML, Sievers RE, Viswanathan MN, Yee MS, Foster E, Grossman W, et al. Closed-chest cell injections into mouse myocardium guided by high-resolution echocardiography. Am J Physiol Heart Circ Physiol. 2005;289(3):H1307-14.
28. Zhang M, Methot D, Poppa V, Fujio Y, Walsh K, Murry CE. Cardiomyocyte grafting for cardiac repair: graft cell death and anti-death strategies. J Mol Cell Cardiol. 2001;33(5):907-21.
29. Deddens JC, Feyen DA, Zwetsloot PP, Brans MA, Siddiqi S, van Laake LW, et al. Targeting chronic cardiac remodeling with cardiac progenitor cells in a murine model of ischemia/reperfusion injury. PLoS One. 2017;12(3):e0173657.
30. Giraldo A, Talavera Lopez J, Fernandez-Del-Palacio MJ, Garcia-Nicolas O, Seva J, Brooks G, et al. Percutaneous Contrast Echocardiography-guided Intramyocardial Injection and Cell Delivery in a Large Preclinical Model. J Vis Exp. 2018(131).
31. Ahmadi A, Thorn SL, Alarcon EI, Kordos M, Padavan DT, Hadizad T, et al. PET imaging of a collagen matrix reveals its effective injection and targeted retention in a mouse model of myocardial infarction. Biomaterials. 2015;49:18-26.
32. Le NT, Dunleavy MW, Zhou W, Bhatia SS, Kumar RD, Woo ST, et al. Stem Cell Therapy for Myocardial Infarction Recovery: Advances, Challenges, and Future Directions. Biomedicines. 2025;13(5).
33. Kurtz A. Mesenchymal stem cell delivery routes and fate. Int J Stem Cells. 2008;1(1):1-7.
34. Sheng CC, Zhou L, Hao J. Current stem cell delivery methods for myocardial repair. Biomed Res Int. 2013;2013:547902.
35. Raval AN, Pepine CJ. Clinical Safety Profile of Transendocardial Catheter Injection Systems: A Plea for Uniform Reporting. Cardiovasc Revasc Med. 2021;22:100-8.
36. Vekstein AM, Wendell DC, DeLuca S, Yan R, Chen Y, Bishawi M, et al. Targeted Delivery for Cardiac Regeneration: Comparison of Intra-coronary Infusion and Intra-myocardial Injection in Porcine Hearts. Front Cardiovasc Med. 2022;9:833335.
37. Yao Y, Ding J, Wang Z, Zhang H, Xie J, Wang Y, et al. ROS-responsive polyurethane fibrous patches loaded with methylprednisolone (MP) for restoring structures and functions of infarcted myocardium in vivo. Biomaterials. 2020;232:119726.

38. Asgari R, Mehran YZ, Weber HM, Weber M, Golestanha SA, Hosseini Kazerouni SM, et al. Management of oxidative stress for cell therapy through combinational approaches of stem cells, antioxidants, and photobiomodulation. Eur J Pharm Sci. 2024;196:106715.
39. Abdel-Farid IB, Sheded MG, Mohamed EA. Metabolomic profiling and antioxidant activity of some Acacia species. Saudi J Biol Sci. 2014;21(5):400-8.
40. Maroyi A. Acacia karroo Hayne: Ethnomedicinal uses, phytochemistry and pharmacology of an important medicinal plant in southern Africa. Asian Pac J Trop Med. 2017;10(4):351-60.
41. More GK, Meddows-Taylor S, Prinsloo G. Metabolomic Profiling of Antioxidant Compounds in Five Vachellia Species. Molecules. 2021;26(20).
42. Njanje I, Bagla VP, Beseni BK, Mbazima V, Lebogo KW, Mampuru L, et al. Defatting of acetone leaf extract of Acacia karroo (Hayne) enhances its hypoglycaemic potential. BMC Complement Altern Med. 2017;17(1):482.
43. Tshikalange TE, Meyer JJ, Hussein AA. Antimicrobial activity, toxicity and the isolation of a bioactive compound from plants used to treat sexually transmitted diseases. J Ethnopharmacol. 2005;96(3):515-9.
44. Chiaino E, Micucci M, Durante M, Budriesi R, Gotti R, Marzetti C, et al. Apoptotic-Induced Effects of Acacia Catechu Willd. Extract in Human Colon Cancer Cells. Int J Mol Sci. 2020;21(6).
45. Adedapo AA. Safety Evaluations of the Aqueous Extract of Acacia karroo Stem Bark in Rats and Mice Records of natural products 2008.
46. Ponath V, Kaina B. Death of Monocytes through Oxidative Burst of Macrophages and Neutrophils: Killing in Trans. PLoS One. 2017;12(1):e0170347.
47. Merck. Phorbol 12-myristate 13-acetate [Available from: https://www.sigmaaldrich.com/BE/en/product/sigma/p8139?utm_source=google&utm_medium=cpc&utm_campaign=22183687420&utm_content=181001661304&gad_source=1&gad_campaignid=22183687420&gbraid=0AAAAAD8kLQRSIfshpIr3Yk9AeXzsfzWGD&gclid=CjwKCAjw3f_BBhAPEiwAaA3K5M69CwbtdE44ttfPVZn3_5kkAfmtKvsLCl0Ju2DL19BL7eqfVpm0EROoCRKgQAvD_BwE.
48. Behnen M, Moller S, Brozek A, Klinger M, Laskay T. Extracellular Acidification Inhibits the ROS-Dependent Formation of Neutrophil Extracellular Traps. Front Immunol. 2017;8:184.

This text was supported by GenAI